Materials Research Letters
Publication details, including instructions for authors and subscription information:
http://www.tandfonline.com/loi/tmrl20

Temperature-Induced Short-Range Order Changes in $Co_{67}B_{33}$ Glassy Thin Films and Elastic Limit Implications

Volker Schnabel[a], Jozef Bednarcik[b], Denis Music[a], Tomas Pazur[a], Carolin Hostert[a] & Jochen M. Schneider[a]

[a] Materials Chemistry, RWTH Aachen University, Kopernikusstr. 10, D-52074 Aachen, Germany

[b] Deutsches Elektronen Synchrotron DESY, FS-PE Group, Notkestrasse 85, D-22607 Hamburg, Germany

Published online: 25 Sep 2014.

To cite this article: Volker Schnabel, Jozef Bednarcik, Denis Music, Tomas Pazur, Carolin Hostert & Jochen M. Schneider (2014): Temperature-Induced Short-Range Order Changes in $Co_{67}B_{33}$ Glassy Thin Films and Elastic Limit Implications, Materials Research Letters, DOI: 10.1080/21663831.2014.963207

To link to this article: http://dx.doi.org/10.1080/21663831.2014.963207

MATERIALS RESEARCH LETTERS

Mater. Res. Lett., 2014
http://dx.doi.org/10.1080/21663831.2014.963207

Taylor & Francis
Taylor & Francis Group

www.tandfonline.com/toc/tmrl20/current

Temperature-Induced Short-Range Order Changes in $Co_{67}B_{33}$ Glassy Thin Films and Elastic Limit Implications

Volker Schnabel[a]*, Jozef Bednarcik[b], Denis Music[a], Tomas Pazur[a], Carolin Hostert[a] and Jochen M. Schneider[a]

[a]*Materials Chemistry, RWTH Aachen University, Kopernikusstr. 10, D-52074 Aachen, Germany;* [b]*Deutsches Elektronen Synchrotron DESY, FS-PE Group, Notkestrasse 85, D-22607 Hamburg, Germany*

(*Received 30 July 2014; final form 3 September 2014*)

In situ high-temperature X-ray diffraction experiments using high-energy photons and *ab initio* molecular dynamics simulations are performed to probe the temperature-induced changes in the topological short-range order in magnetron sputtered $Co_{67}B_{33}$ metallic glass thin films. Based on this correlative experimental and theoretical study, the presence of B–Co–B rigid second-order structures at room temperature and the temperature-induced decrease in the population of these strongly bonded building blocks are inferred. This notion is consistent with experimental reports delineating the temperature dependence of elastic limit.

Keywords: Metallic Glasses; Strength; Synchrotron; XRD; PVD

Introduction Co-based metallic glasses are amorphous solids with a high degree of topological and chemical short-range order [1] which exhibit fascinating structural and functional properties.[2] For example, Co–Fe–Ta–B-based bulk metallic glasses have an extremely high maximum permeability of 500,000 and very low coercivity of 0.26 A/m.[2] Due to such excellent soft magnetic properties Co,Fe-based bulk metallic glasses show great potential for consolidated magnetic cores for power supply applications.[3] Also, Inoue et al. [4] report with $>5{,}000$ MPa a very large elastic limit. The combination of the high elastic limit and the smooth surface render these metallic glasses suitable for micro components, for example, micro gears for high-precision endoscopes.[2,5] Furthermore, Co,Fe-based bulk metallic glasses show a strong temperature-dependent elastic limit from the ultra-high strength of 5,185 MPa at room temperature to 1,100 MPa at 873 K, while the elastic modulus of 268 GPa appears to be preserved.[4] Mechanical properties of metallic glasses at elevated temperatures have been investigated by a small sample compression test [4,6] or extrusion.[7] Furthermore, the temperature-dependent short-range order has been studied by high-energy X-ray diffraction (XRD) [8,9] or molecular dynamic (MD) simulation.[10–12] However, no correlative discussion of the temperature-induced changes in the short-range order and mechanical properties can be found in the literature. The very high stiffness of Co,Fe-based metallic glasses at room temperature is according to Wang et al. [13] and Hostert et al. [14] caused by the presence of strong, covalent Co–B and (Co,Fe)–B bonds, respectively.

Since temperature-induced changes in topology and/or chemical ordering have not been investigated by theoretical or by experimental means the underlying cause of the strong temperature dependence of the elastic limit in Co,Fe-based bulk metallic glasses is unknown. The objective of this work is to identify the temperature-induced topological evolution of the $Co_{67}B_{33}$ metallic glass thin films, to enable knowledge-based design of new metallic glasses with high strength and plasticity at room temperature. To this end, we employ *in situ* high-temperature, high-energy XRD experiments [9] in combination with *ab initio* MDs simulations.[14]

Experimental Methods $Co_{67}B_{33}$ metallic glass thin films were synthesized by magnetron sputtering, using a ultra-high vacuum system with a base pressure of

*Corresponding author. Email: schnabel@mch.rwth-aachen.de

$4 \cdot 10^{-5}$ Pa. Elemental targets, with a diameter of 2 in. and a purity of 99.95% for cobalt and 99.5% for boron were used. For cobalt and boron direct current and radio frequency power supplies were utilized, respectively. The target power densities were set to be 1.6 W cm^{-2} for cobalt and 8.4 W cm^{-2} for boron. During deposition, the argon partial pressure was 0.4 Pa. The target to substrate distance was 10 cm and the substrate holder was rotated with 30 rpm. As a substrate, polycrystalline sodium chloride was used, which was later removed from the metallic glass thin film by rinsing it with demineralized water, acetone and methanol. The deposition time was 6 h, resulting in a film thickness of 3 µm. The chemical composition and purity of the so obtained thin film powder was analysed by standard less energy dispersive X-ray analysis at an acceleration voltage of 4 kV using a JEOL, JSM-6480 scanning electron microscope equipped with an EDAX detector performing a background, atomic number, absorption and fluorescence correction.

In situ high-energy, high-temperature XRD experiments were performed in transmission geometry using a Linkam THMS 600 heating stage. The separated metallic glass thin film sample was put into a quartz capillary with a wall thickness of 20 µm and a diameter of 1 mm. The sample was heated from room temperature up to 863 K at a heating rate of 10 K/min. Heating was done under protective Ar atmosphere. The sample was instantaneously illuminated with a monochromatic photon beam (wavelength $\lambda = 0.02073$ nm). Diffracted photons were recorded with a fast image plate detector Perkin Elmer 1621. Two-dimensional XRD patterns were acquired every 12 s. The sample-to-detector distance was set to 32.3 cm. Due to heater geometry, the maximum wave vector q was limited to 14 Å^{-1}.

Two-dimensional XRD patterns were integrated to the q-space using the software package FIT2D.[15] These data were then converted to the total structure factor, $S(q)$, using standard procedures described elsewhere.[14,16] The integrated data were corrected for sample absorption, fluorescence contribution and inelastic (Compton) scattering. The total structural factor $S(q)$ was obtained from the normalized elastically scattered intensity. The pair distribution functions (PDFs) were obtained from the structure factor through a sine Fourier transform using standard procedures described elsewhere.[14]

Theoretical Methods *Ab initio* MD simulations based on density functional theory,[17] using a canonical ensemble were performed to enable a structure analysis as a function of temperature. The simulations were performed using the OpenMX code,[18] applying electronic potentials with the generalized gradient approximation and basis functions in the form of linear combination of localized pseudo-atomic orbitals.[19,20] Co5.5-s2p1d1 and B4.5-s2p2 were used as basic functions. The first symbol denotes the chemical name, followed by the cut-off radius and the set of primitive orbitals applied. The energy cut-off of 150 Ry and N-point grid of 72 × 72 × 72 was used.

A disordered configuration was obtained by heating the super cell at 4,000 K for 400 fs, by scaling the velocity. For this initial configuration, the method of Hostert et al. [14] was applied. The initial configuration was a body centre cubic super cell with 128 lattice sites. On these 128 lattice sites, 115 atoms were placed randomly, thereby yielding to a composition of $Co_{67}B_{33}$ and 13 vacancies.[14] Afterwards, the super cell was quenched to 2,000 K and held at this temperature for 1,000 fs. Thereafter, a stepwise structure analysis was performed. The temperature step size was chosen to be 100 K and the time held at each step was 500 fs. This yields in an approximate cooling rate of $2 \cdot 10^{14}$ K/s. For the structural analysis, the last 250 fs of each temperature step was taken into account. The MD time step was set to 1 fs. The topological evolution was examined by calculating total and partial PDFs, bond angle distribution and Voronoi tessellation.

Based on Voronoi tessellation, the atom-specific nearest neighbour coordination was estimated [21] by utilizing the atomic coordinates of the relaxed *ab initio* MD data as input, defining the configuration for each temperature. In this work, the radical plane method was applied, which takes the atomic radii of the atoms into account.[22] When projected planes meet, edges and consequently faces of polyhedra are formed. These polyhedra are described by the Voronoi index [n_3, n_4, n_5, n_6], where n_i denotes the number of i-edged faces of the Voronoi polyhedron. For the analysis and visualization of OpenMX data, the 'Atomic structure analysis package' [23] was used.

Results and Discussion The temperature-induced topology evolution is initially examined by comparing the PDFs obtained from *in situ* high-energy, high-temperature XRD experiments with the PDFs simulated with *ab initio* MD. Figure 1 shows a series of the structure factors of the $Co_{67}B_{33}$ powder as a function of temperature in a three-dimensional plot at the top and a colour intensity plot at the bottom. A common feature for the structure factors below 758 K is that they exhibit broad principal peak located at 3.21 Å^{-1} followed by rather broad peaks of rapidly decaying intensity towards larger q-values. This is a fingerprint of missing long-range order in the material studied and confirms its fully amorphous nature. However, the number as well as the intensity of the individual structure factor peaks drastically increase at 758 K as crystallization of the $Co_{67}B_{33}$

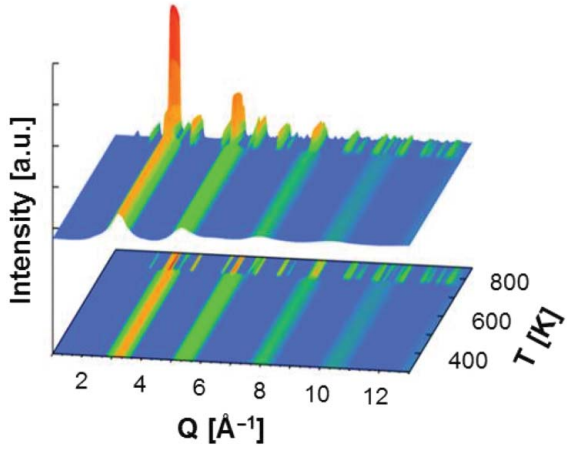

Figure 1. Structure factor of $Co_{67}B_{33}$ as a function of temperature (T) measured by *in situ* high-temperature XRD.

metallic glass powder sets in. The structure of the crystallized material is consistent with the stoichiometric Co_2B phase (JCPDS 25–0241). Hence, the onset of crystallization for $Co_{67}B_{33}$ is at 758 K, which is lower than the crystallization temperatures of quaternary Co–Fe–Ta–B bulk metallic glasses, which have been reported to be in the range of 940–980 K.[4,24] This is expected as it is known that for binary systems as compared to systems with a larger number of components, the number of possible local atomic configurations is lower leading to a decrease in glass stability.[3]

In Figure 2, the PDFs obtained by XRD experiments and MD simulations at selected temperatures are shown. All the PDFs discussed describe the order prior to crystallization (see Figure 1). Comparing the experimental PDFs with the ones obtained by MD simulation, one can see that all main features, such as the peaks' heights and their positions, are in very good agreement. Hence, the computational methodology based on Hostert et al. [14] and Music et al. [23] appears to be useful to describe the temperature-dependent topology of Co–B metallic glass thin films. In Figure 2, the first structural peak at 1.98 Å corresponds to the first coordination shell of Co–B interatomic bond length distribution, which is learned from the partial PDFs obtained by *ab initio* MD (see Figure 3). The second peak at 2.55 Å corresponds to the first Co–Co coordination shell. The amplitude of Co–Co bond length distribution is higher compared to Co–B bond length distribution, which is due to the larger weighting factor of cobalt compared to boron. Furthermore, there are no distinct features of B–B bonds visible in the total PDFs shown in Figure 2. Peaks at distances larger than 2.55 Å can be attributed to the second and third coordination shells. The position of the first bond length distribution maxima does not change by increasing the temperature from 300 to 700 K. The bond length distribution of the second coordination shell is characterized

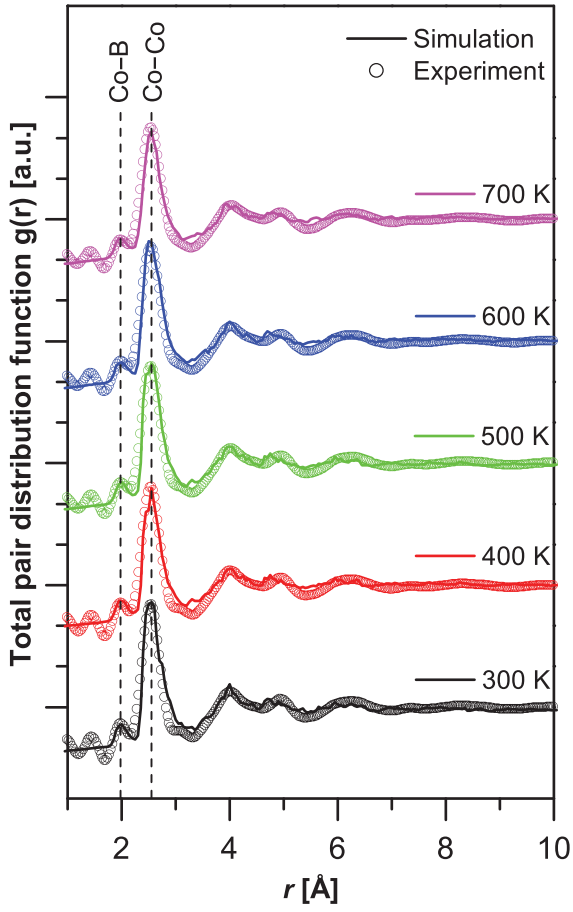

Figure 2. Comparison between the *in situ* measured and *ab intio* MDs, total pair distribution data in the temperature range of 300–700 K. For better comparison, curves are vertically offset.

by two, equally temperature independent maxima at 4 and 5 Å, which according to Waal [25] may imply some spatial orientation coherence between the first and second coordination shell as well as the presence of dense tetrahedral packing.[26]

From the investigation of the structure factors and the total PDFs, we observe very good agreement between theory and experiment. However, no cause of the experimentally observed temperature-dependent mechanical behaviour could be identified as all total PDFs, which are dominated by Co–Co interactions appear to be temperature independent.

To probe the temperature-induced changes in structure further, the partial PDFs obtained by *ab initio* MD simulation shown in Figure 3 are examined. In an attempt to overcome the limitations posed by the extensive simulation time requirements during *ab initio* MD simulations,[27] the analysis of partial PDFs obtained at temperatures exceeding the experimentally studied temperature range is performed.

On the left side of Figure 3, the partial Co–B PDFs are shown in a temperature range of 300–1,600 K. For

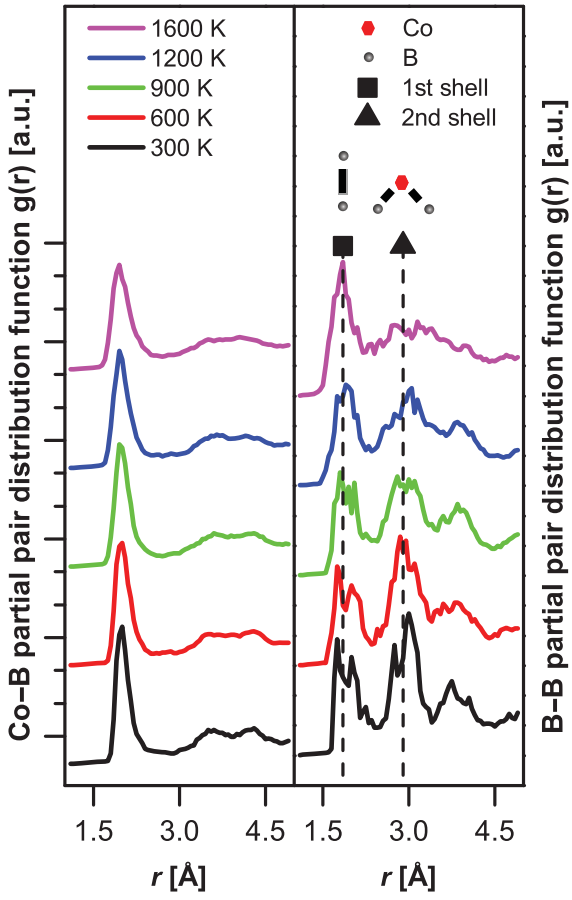

Figure 3. The atomic Co–B (left panel) and B–B (right panel) partial PDF data obtained by *ab inito* MDs simulation in the temperature range of 300–1,600 K are shown. The vertical lines correspond to the square and the triangular symbol indicates the location of the first and second B–B coordination shell, respectively.

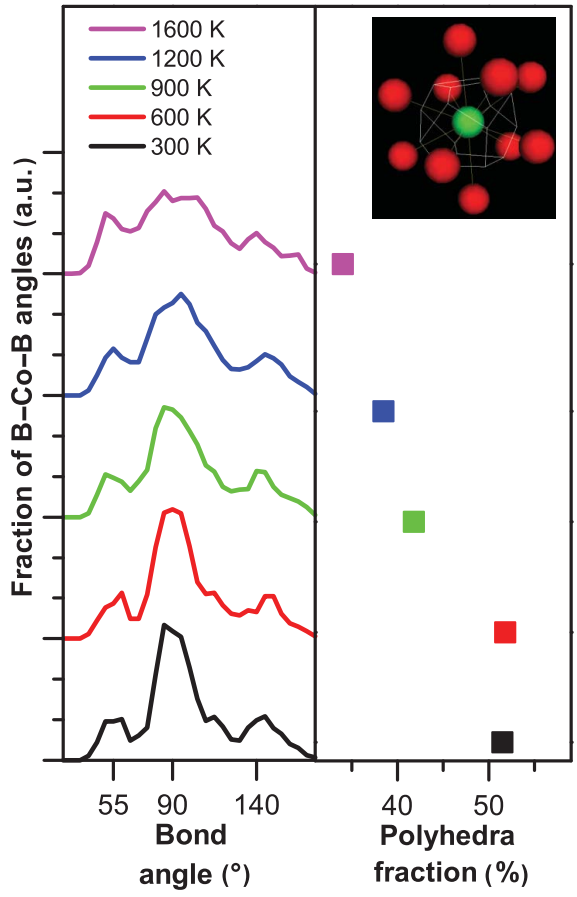

Figure 4. The bond angle distribution of the B–Co–B bonds in the temperature range of 300–1,600 K obtained by *ab initio* MDs simulation is shown (left panel). The fraction of Frank–Kasper-like Voronoi polyhedra is shown in the same temperature range (right panel). Furthermore, an example of the most dominant boron-centred bicapped square Archimedean antiprism, with the Voronoi index of (0,2,8,0), is given in the upper right corner.

the partial PDFs, the *r*-range shown is 1–5 Å. The first peak at 1.98 Å corresponds to the first coordination shell of Co–B pairs. With a deviation of 1% such bond length is in good agreement with the Co–B bond distance as observed in the case of the quaternary Co–Fe–Ta–B metallic glass.[14] With increasing temperature, the peak broadens and its amplitude decreases, which is due to a wider distribution of Co–B bond lengths. At 300 and 600 K, the second peak and the third peak corresponding to the second coordination shell of Co–B bond length exhibit maxima at 3.5 and 4.3 Å, respectively. The two peaks broaden and finally merge as the temperature is increased, which can be explained by the loss of coherence between the first and second Co–B coordination shell.[25]

On the right side of Figure 3, the B–B partial PDFs from the temperature range of 300–1,600 K are shown. At room temperature, there are three peaks visible, whereas at 1,600 K, the B–B partial PDF is dominated by the first peak as the second peak and the third peak have merged to a broad peak which is strongly reduced in amplitude. The first B–B coordination shell, which corresponds to the first peak at 1.85 Å, is indicated by squares. The distance of the second B–B coordination shell (indicated by triangles) is 2.9 Å. At room temperature, the second B–B coordination shell shows a higher amplitude than the peak of the first coordination shell. This observation is consistent with other boron-containing metallic glass systems.[10,26] It is evident that the partial distribution functions of both B–B and Co–B are strongly affected by temperature. However, at this point, it is unclear which building blocks can be associated with the decrease in bond length distribution amplitude that has been observed as the temperature is increased.

To determine which building block(s) can be associated with the second B–B peak, the angular distribution of the B–Co–B structure is examined. On the left side of Figure 4, the angular distribution of B–Co–B bonds in

the temperature range of 300–1,600 K is shown. For all temperatures, there are three peaks visible at 55°, 90° and 140°. The peak at 90° shows the largest fraction of B–Co–B bond angles for all temperatures. However, the peak at 90° broadens, indicating a population density decrease as the temperature is increased. From the partial PDFs shown in Figure 3, one can learn that the first Co–B shell distance is equal to 1.98 Å at 300 K. B–Co–B structures with a Co–B distance of 1.98 Å and a bond angle of 90°, result in B–B distance of 2.82 Å. This value is in very good agreement with the second coordination shell distance obtained in the calculation of the B–B partial distribution function shown in Figure 3. Therefore, it is evident from the correlative analysis of the partial distribution functions and the bond angle distribution data that the population of B–Co–B building blocks with a 90° bond angle that are present at room temperature is drastically reduced as the temperature is increased. It is reasonable to assume that this temperature-induced decrease in the population of covalently bonded [13,14] and therefore stiff B–Co–B building blocks has implications for the mechanical properties: as mentioned earlier, the elastic limit of Co-based metallic glasses shows a strong temperature dependence.[4] According to Inoue et al.,[4] the elastic limit of $Co_{43}Fe_{20}Ta_{5.5}B_{31.5}$ drops by 80% as the temperature is increased from room temperature to 873 K. The temperature dependence of the elastic limit is consistent with the temperature-induced loss of coherence between the first and second Co–B coordination shell and the temperature-induced decrease in the population of stiff B–Co–B building blocks, which is inferred from the partial PDFs and the B–Co–B bond angle analysis. Even though there is a difference in absolute temperature between the experimentally observed drop in elastic limit [4] and the observed loss of coherence between the first and second Co–B coordination, the inferred topology evolution provides insight towards designing high strength (Co,Fe)-based metallic glasses. This difference may be due to the different chemistry, sample size or limitations posed by the extensive simulation time requirements towards relaxation.

It is proposed by Zhang et al. [28] that plastic behaviour is promoted by decreasing the fraction of Frank–Kasper-like polyhedra. With a decrease in the fraction of densely packed polyhedra the fraction of ready-to-flow region increases, which on the one hand promotes plastic behaviour and on the other hand decreases the chance for severe shear localization.[28] An increase in ready-to-flow regions may cause a change in deformation mode from shear band-dominated mode to homogeneous deformation mode as it is seen for many metallic glasses.[4,29,30] On the right side of Figure 4, the fraction of densely packed cobalt- and boron-centred Frank–Kasper-like Voronoi polyhedra is shown in the temperature range of 300–1,600 K. The most dominant polyhedron at 300 K is the boron-centred bicapped square Archimedean antiprism (Figure 4), with the Voronoi index of (0,2,8,0). Hence, the boron-centred short-range order present in the crystalline phase is also present in the glass structure. In contrast to the crystalline phase, in which every boron atom has the same short-range order only 12% of the boron-centred polyhedra in the glass have that particular coordination. The fraction of densely packed Frank–Kasper-like cobalt- and boron-centred polyhedra decreases from 50% at 300 K to about 35% at 1,600 K. This implies a significant increase in the fraction of ready-to-flow regions as the temperature is increased,[28] which is consistent with the experimentally observed drop in elastic limit.[4] The temperature-induced decrease in the population of Frank–Kasper-like polyhedra is also consistent with above presented notion on the temperature-induced loss of coherence between the first and second Co–B coordination shell and the structural changes derived by the partial PDFs.

A key issue in designing ductile metallic glasses is controlling shear band nucleation and propagation.[31] The here reported temperature-induced changes in the topological and chemical order cause an increase in the population of ready-to-flow regions, which facilitates a ductile behaviour.[4] Future materials design strategies may focus on decreasing structural coherence between the first and second coordination shell, by alloying to stabilize ready-to-flow regions at lower temperatures.

Conclusions *In situ* high-temperature XRD experiments using high-energy photons and *ab initio* MDs simulations are performed to probe the temperature-induced changes in the topological short-range order in magnetron sputtered $Co_{67}B_{33}$ metallic glass thin films. Good agreement between the experimentally obtained PDFs and the PDFs obtained by *ab initio* MD simulation is observed. The loss in coherence between the first and second Co–B coordination shell together with the evolution of the B–B coordination is inferred based on the observed temperature-induced decrease in the population of rigid second-order B–Co–B building blocks. This interpretation is also consistent with the thermally induced decrease in the population of densely packed Frank–Kasper-like polyhedra, which was obtained by Voronoi tessellation. The here reported temperature-induced changes in the topological and chemical order cause an increase in the population of ready-to-flow regions inferring a transition from a localized shear band-dominated deformation mode to a homogeneous deformation mode, which may explain the extensive temperature dependence of the elastic limit reported previously. The here reported temperature-induced changes in the topological and chemical order may be exploited in future materials design efforts to enhance the ductility

of these very stiff solids stabilizing ready-to-flow regions at lower temperature by alloying.

Acknowledgements This work was supported by the Deutsche Forschungsgemeinschaft within the [SPP-1594] 'Quantum mechanically guided design of ultra strong glasses'.

References

[1] Kaban I, Jovari P, Stoica M, Eckert J, Hoyer W, Beuneu B. Topological and chemical ordering in $Co_{43}Fe_{20}Ta_{5.5}B_{31.5}$ metallic glass. Phys Rev B. 2009;79:212201.

[2] Inoue A, Shen B, Takeuchi A. Developments and applications of bulk glassy alloys in late transition metal base system. Mater Trans. 2006;47:1275–1285.

[3] Inoue A. Stabalization of metallic supercooled liquid and bulk amorphous alloys. Acta Mater. 2000;48:279–306.

[4] Inoue A, Shen BL, Koshiba H, Kato H, Yavari AR. Ultra-high strength above 5000 MPa and soft magnetic properties of Co-Fe-Ta-B bulk glassy alloys. Acta Mater. 2004;52:1631–1637.

[5] Ishida M, Takeda H, Watanabe D, Amiya K, Nishiyama N, Kita K, Saotome Y, Inoue A. Fillability and imprintability of high-strength Ni-based bulk metallic glass prepared by the precision die-casting technique. Mater Trans. 2004;45:1239–1244.

[6] Lu J, Ravichandran G, Johnson WL. Deformation behavior of the Zr41.2Ti13.8Cu12.5Ni10Be22.5 bulk metallic glass over a wide range of strain-rates and temperatures. Acta Mater. 2003;51:3429–3443.

[7] Shao Z, Gopinadhan M, Kumar G, Mukherjee S, Liu Y, O'Hern CS, Schroers J, Osuji CO. Size-dependent viscosity in the super-cooled liquid state of bulk metallic glass. Appl Phys Lett. 2013;102:221901.

[8] Mattern N, Bednarcik J, Stoica M, Eckert J. Temperature dependence of the short-range order of $Cu_{65}Zr_{35}$ metallic glass. Intermetallics. 2013;32:51–56.

[9] Michalik S, Gamová J, Bednarcik J, Varga R. In situ structural investigation of amorphous and nanocrystalline $Fe_{40}Co_{38}Mo_4B_{18}$ microwires. J Alloy Compd. 2011;509:3409–3412.

[10] Qin J, Gu T, Yang L. Structural and dynamical properties of $Fe_{78}Si_9B_{13}$ alloy during rapid quenching by first principles molecular dynamic simulation. J Non-Cryst Solids. 2009;355:2333–2338.

[11] Xia JH, Cheng ZF, Shi DP, Xiao X. A molecular dynamics study of structural transition of Ti during the rapid quenching process. Physica B. 2012;407:2112–2118.

[12] Lewis LJ, Vita AD. Structure and electronic properties of amorphous indium phosphide from first principles. Phys Rev B. 1998;57:1594–1606.

[13] Wang J, Li R, Xiao R, Xu T, Li Y, Liu Z, Huang L, Hua N, Li G, Li Y, Zhang Y. Compressibility and hardness of Co-based bulk metallic glass: a combined experimental and density functional theory study. Appl Phys Lett. 2011;99:151911.

[14] Hostert C, Music D, Bednarcik J, Keckes J, Kapaklis V, Hjörvarsson B, Schneider JM. *Ab initio* molecular dynamics model for density, elastic properties and short range order of Co-Fe-Ta-B metallic glass thin films. J Phys Condens Mat. 2011;23:475401.

[15] Hammersley AP, Svensson SO, Hanfland M, Fitch AN, Häusermann D. Two-dimensional detector software: from real detector to idealised image or two-theta scan. High Pressure Res. 1995;14:235–248.

[16] Egami T, Billinge SJL. Underneath the Bragg peaks: structural analysis of complex materials. Oxford: Elsevier; 2003.

[17] Hohenberg P, Kohn W. Inhomogeneous electron gas. Phys Rev. 1964;136:864–871.

[18] Ozaki T, Kino H. Efficient projector expansion for the *ab initio* LCAO method. Phys Rev B. 2005;72:045121.

[19] Sholl DS. Density functional theory: a practical introduction. Hoboken, NJ: Wiley; 2009.

[20] Ozaki T. Variationally optimized atomic orbitals for large-scale electronic structures. Phys Rev B. 2003;67: 155108.

[21] Finney JL. Random packings and the structure of simple liquids I. The geometry of random close packing. Proc R Soc Lon Ser A. 1970;319:479–493.

[22] Park J, Shibutani Y. Common errors of applying the Voronoi tessellation technique to metallic glasses. Intermetallics. 2012;23:91–95.

[23] Music D, Hensling F, Pazur P, Bednarcik J, Hans M, Schnabel V, Hostert C, Schneider JM. Bonding and elastic properties of amorphous $AlYB_{14}$. Solid State Commun. 2013;169:6–9.

[24] Taghvai AH, Stoica M, Khoshkhoo MS, Kaban I, Bednarcik J, Jóvári P, Janghorban K, Eckert J. DSC, XRD and TEM characterization of glassy $Co_{40}Fe_{22}Ta_8B_{30}$ alloy with very high thermal stability. Mater Lett. 2013;93:322–325.

[25] Waal BWVD. On the origin of second-peak splitting in the static structure factor of metallic glasses. J Non-Cryst Solids. 1995;189:118–128.

[26] Hui X, Lin DY, Chen XH, Wang WY, Wang Y, Shang SL, Liu ZK. Structural mechanism for ultrahigh-strength Co-based metallic glasses. Scripta Mater. 2013;68:257–260.

[27] Frauenheim T, Seifert G, Elstner M, Niehaus T, Köhler C, Amkreutz M, Sternberg M, Hajnal Z, Carlo AD, Suhai S. Atomistic simulations of complex materials: ground-state and excited-state properties. J Phys Condens Matter. 2002;14:3015–3047.

[28] Zhang L, Cheng Y, Cao A, Xu J, Ma E. Bulk metallic glasses with large plasticity: composition design from the structural perspective. Acta Mater. 2009;57:1154–1164.

[29] Schuh CA, Lund AC, Nieh TG. New regime of homogeneous flow in the deformation map of metallic glasses: elevated temperature nanoindentation experiments and mechanistic modeling. Acta Mater. 2004;52:5879–5891.

[30] Li L, Wang N, Yan F. Transient response in metallic glass deformation: a study based on shear transformation zone dynamics simulations. Scripta Mater. 2014;80:25–28.

[31] Greer AL, Cheng YQ, Ma E. Shear bands in metallic glasses. Mater Sci Eng, R. 2013;74:71–132.